ACS Catalysis

Review

pubs.acs.org/acscatalysis

Ketonization of Carboxylic Acids in Biomass Conversion over TiO_2 and ZrO_2 Surfaces: A DFT Perspective

Gianfranco Pacchioni*

Dipartimento di Scienza dei Materiali, Università di Milano-Bicocca, Via R. Cozzi, 55, I-20125 Milano, Italy

ABSTRACT: Carboxylic acids play a fundamental role in the transformation of biomass into liquid fuels and other useful chemicals. In order to reduce the O/C content of biofuels, carboxylic acids need to be decomposed by decarboxylation, dehydroxylation, or decarbonylation unimolecular reactions, or they need to be converted into ketones via complex bimolecular reaction mechanisms. Ketonization, that is, the transformation of carboxylic acids into ketones, carbon dioxide, and water, is promoted by heterogeneous catalysts based on oxide materials. Among the most active catalysts are titania and zirconia surfaces. In recent years, a large body of experimental data has been complemented by specific investigations performed with first-principles electronic structure calculations based on density functional theory (DFT). In this review, I discuss the present level of understanding of the bonding modes of carboxylic acids (acetic acid in particular) on the TiO_2 and ZrO_2 surfaces as obtained from DFT calculations. Enolization and ketonization reaction mechanisms determined at the DFT level on TiO_2 and ZrO_2 surfaces are also discussed, and the results are analyzed in view of the experimental evidence. Finally, the role of supported metal particles, of the redox properties of the oxide catalyst, and the nature of the active sites on the surface of titania and zirconia are discussed.

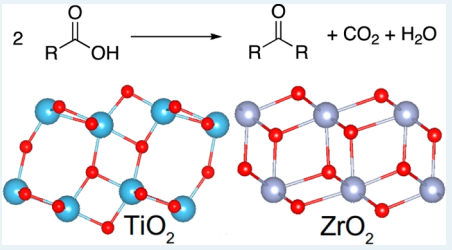

KEYWORDS: *density functional theory, carboxylic acids, ketonization, biofuels, TiO_2, ZrO_2*

1. INTRODUCTION

Lignocellulosic biomass from agriculture and forestry is an important raw material for the production of biofuels. Conversion of lignocellulose into fuels has been attempted by a number of different routes but is not simple due to the chemical complexity of lignocellulose, the elevated stability, and the high oxygen content. The production of liquid fuels from lignocellulose requires to decrease the O/C ratio (by removal of oxygen) and to increase the H/C ratio (by the addition of hydrogen). The conversion of large volumes of solid biomass to liquids is largely done via pyrolysis,[1] a process where biomass is treated under inert atmosphere to yield gases, liquids (bio-oil), and a solid residue. Bio-oil contains 15−25% in weight of water, more than 40% in weight of oxygen, and has a very complex composition (up to 400 different components have been identified[2]). For these reasons the bio-oil is subjected to upgrading treatments[3] to improve its physicochemical properties. Catalytic pyrolysis is an interesting alternative to convert lignocellulosic biomass into fuels. In recent years, a variety of catalytic treatments, based on condensation reactions between oxygen-containing groups, have been investigated in order to reduce the oxygen content of bio-oil.[4]

Among the components of biofuels are carboxylic acids, which play a fundamental role in the transformation of biomass.[5] The thermal deoxygenation of carboxylic acids is an important step in the conversion of biomass into aliphatic hydrocarbons that form the basis of biofuels. Decarboxylation reaction 1 is a primary decomposition pathway under pyrolysis conditions. It represents an ideal conversion process because it eliminates two oxygens for every carbon atom removed:

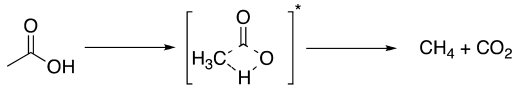

(1)

The unimolecular decomposition of acetic acid (CH_3COOH), and in general of carboxylic acids, can also occur via dehydration, leading to the formation of water and a ketene derivative (RR′C═C═O), reaction 2:

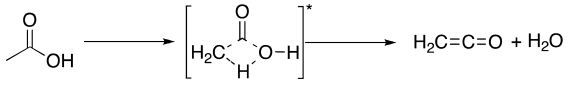

(2)

For acids containing α-hydrogens (i.e., the hydrogen bonded to a carbon atom in the α position relative to a carbonyl group) dehydration may also proceed through a two-step process in which a hydrogen atom transfers from the α-carbon to the carbonyl oxygen to form an 1,1-enediol, as shown in reaction 3a. This reaction can be followed by the elimination of a water molecule to form a ketene derivative, as depicted in reaction 3b:

Received: June 9, 2014
Revised: July 16, 2014
Published: July 18, 2014

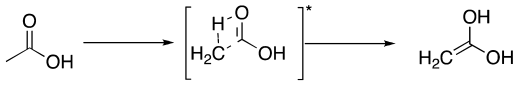
(3a)

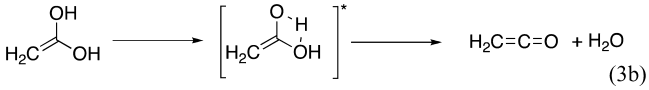
(3b)

When acetic acid is adsorbed on metal oxides, two other reactions can occur, chemical reduction with formation of acetaldehyde (CH_3CHO), and ketonization which leads to the formation of acetone (CH_3COCH_3).[5] Differently from reactions 1−3, unimolecular, ketonization is a bimolecular process in which two molecules of a carboxylic acid are coupled to produce a symmetric ketone, forming a CO_2 and an H_2O molecule during the process,[5,6] see reaction 4:

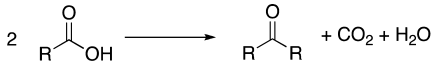
(4)

Ketonization of carboxylic acids is a well-known reaction in organic chemistry.[7] The mechanisms and the catalysts used for this reaction have been recently summarized and discussed in the excellent review article by Pham et al.[8] There are two types of ketonization reactions, bulk ketonization, which occurs via decomposition of carboxylate salts, and surface ketonization which is catalyzed by oxide surfaces or by zeolites. Thermodynamically, ketonization is more favorable than dehydration.[6] For instance, the dehydration of the acetic acid to produce ketene ($CH_2{=}C{=}O$) (reactions 2 and 3) has an enthalpy of reaction of 32 kcal/mol, whereas the ketonization of acetic acid to produce acetone, reaction 4, has an enthalpy of reaction of only 4 kcal/mol.[9] Decarboxylation, reaction 1, with formation of CO_2 and methane is exothermic with a $\Delta H = -10.0$ kcal/mol. These values are well reproduced by high quality quantum chemical calculations.[10] Finally, decarbonylation, with direct loss of CO and formation of a C_{n-1} alcohol, represents yet another possible mechanisms for decomposition of organic acids.

All these reaction channels are possible, and the selectivity of the reaction depends on various effects. A particularly important role is that of the oxide surface, when the reaction occurs on an heterogeneous catalyst.[5,6] The unimolecular decarboxylation and dehydration reactions (1−3) involve bond-scission of individual acetate intermediates on the surface. The availability of oxygen from the metal oxide lattice influences the selectivity of these reactions: in general, the less reducible the oxide, the higher the selectivity toward dehydration.[5]

The ketonization reaction 4 is well-known to occur over several polycrystalline oxides,[11] including γ-Al_2O_3,[12] MgO,[13] Fe_3O_4,[14] Fe_2O_3,[14,15] TiO_2,[15,16] ZrO_2,[17] and so forth (Table 1). Notice that at low temperature (573 K) practically no oxide is active in the conversion of acetic acid to acetone; at 673 K, some oxides remain basically inert (e.g., WO_3, SiO_2), whereas others are very active with conversion rates close to 100% (MnO_2, CeO_2).[11] A more recent analysis of the oxide catalysts that promote ketonization of carboxylic acids with different carbon chains, and of the corresponding yield and selectivity can be found in the review by Renz.[18] The rationalization of the behavior of the different oxide surfaces is not straightforward. Currently, two main mechanisms for formation of ketones from carboxylic acids are considered and are based either on Eley−Rideal[19] or on Langmuir−Hinshelwood concepts.[20,21] The former mechanism involves the interaction of a molecule adsorbed on the catalyst surface with a molecule from the gas phase, although the latter mechanism involves the interaction of two molecules adsorbed on the catalyst surface and is by far the more generally accepted mechanism.

Table 1. Activity of Various Oxides (10 wt % MO_x/SiO_2) in Catalytic Conversion of Acetic Acid to Acetone (Adapted from Ref 11)

	yield of acetone (%)	
catalyst	573 K	673 K
SiO_2	2	5
B_2O_3	2	3
MoO_3	2	5
WO_3	2	5
P_2O_5	1	12
V_2O_5	3	21
Bi_2O_3	10	18
NiO	7	
Al_2O_3	0	37
CuO	5	39
ZnO	6	33
PbO	6	76
Cr_2O_3	1	39
Fe_2O_3	13	59
CoO	13	63
MgO	7	59
Nd_2O_3	3	61
La_2O_3	3	87
MnO_2	18	96
CdO	6	94
CeO_2	9	97

Despite the long history of this reaction, the mechanism of ketonization of carboxylic acid is still matter of debate, and no general consensus has been reached yet. Several proposals exist in the literature[5,6,18,8] and include the following:

1. A β-keto acid intermediate (CH_3COCH_2COOH) forms from two monodentate carboxylates via α-hydrogen abstraction. The α-hydrogen abstraction of the adsorbed carboxylate results in formation of an anion which then reacts with a neighboring carboxylate or acyl to produce a β-keto acid. The ketone is formed by decarboxylation of this intermediate. Due to the rapid decomposition, the detection of the β-keto acid intermediate has never been realized. This mechanism cannot explain the formation of ketones from acids that do not possess any α-hydrogen atoms but at the moment is the most widely accepted mechanism.
2. An intermediate forms from two adsorbed molecules of carboxylic acid bound to different active sites or bound to the same cation.[5,16]
3. Recently, it has been suggested that an adsorbed carboxylic acid can be enolized. In this case, the participation of the α-hydrogen is not via the abstraction from the basic oxygen of the surface, but it follows a keto−enol tautomerization step that converts the surface carboxylate into a surface enolate (intramolecular transfer of the α-hydrogen).[22]
4. Formation of an acid anhydride intermediate $(CH_3CO)_2O$ that loses CO_2 to produce the ketone has been proposed to explain the formation of cyclic ketones from dicarboxylic acids.[2]

dx.doi.org/10.1021/cs500791w | ACS Catal. 2014, 4, 2874−2888

5. A ketene intermediate forms and then reacts with a carboxylate to produce the ketone.[12,15]

The mechanistic aspects of this reaction have been discussed by Pham et al.[8] A first observation that emerges from this study is the role of α-hydrogen. A large part of the published ketonization studies seem to agree on the required participation of α-hydrogen. This aspect will be further discussed below in connection to some DFT studies. A second conclusion of the review by Pham et al.[8] is connected to the role of the oxide support. Adsorption of carboxylic acids on oxide surfaces gives rise to carboxylate species, usually bidentate in a bridge position over two surface cations. By thermal treatment the adsorbed carboxylates convert into ketones. On the basis of surface science studies, it has been concluded that an important requirement for ketonization is the presence of specific active sites on the surface: (i) coordinatively unsaturated metal cations/oxygen anions for the initial deprotonation of carboxylic acids; (ii) the existence of surface cations that can bind multiple carboxylates or of pairs of adjacent exposed cations for coupling two carboxylate molecules to produce ketones.

Experiments performed by Kim and Barteau on titania single-crystal surfaces have been very influential in establishing one of the widely accepted mechanisms for ketonization.[16] This is one of the few studies performed on this reaction on a single crystal surface. Carboxylate ketonization was reported to occur on the TiO_2 (001)−{114} faceted surface,[16] which is characterized by the presence of surface cations with two coordination vacancies. The activity has been ascribed to these sites on which a pair of carboxylates are supposed to bind to a common cation:[5]

The coordination of adsorbed carboxylates, produced by dissociative adsorption of carboxylic acids, requires the presence of Brønsted basic sites on the surface. Basic sites are also required to perform the α-hydrogen abstraction, a key step in the reaction. An adjacent Lewis acid (a coordinatively unsaturated cation site) is needed to stabilize and activate another carboxylic acid for the coupling reaction. Thus, the presence of adjacent Lewis acid and Brønsted basic sites seems to be the key for the ketonization reaction on oxide surfaces.

Pham et al.[8] also concluded that the bulk redox ability of the oxide may correlate with the ketonization activity, because the redox properties are strongly linked to the acid−base properties of the solid and the ability to expose surface cations. This point, and the role of supported metal particles in the enhancement of the activity of the oxide material, still need a more detailed analysis at an atomistic level and will be further discussed below (see section 7).

Quantum chemistry, and in particular DFT approaches, can complement the abundant experimental information existing on ketonization reactions. Compared to the large number of catalytic studies in this field, the number of theoretical investigations is surprisingly small. In the following, I will discuss adsorption modes of carboxylic acids on the surfaces of TiO_2 and ZrO_2, two oxides commonly used in ketonization reactions. I will analyze in detail some examples of theoretical studies of the reaction mechanism of carboxylic acids on oxide surfaces, like enolization and ketonization, and I will consider the role of supported metal particles in the adsorption and reaction of carboxylic acids on oxides. It is worth mentioning that the chemistry and the mechanism of the reaction when Fe oxides and MgO are used as catalysts can be quite different, because their chemical properties are very different compared to Ti and Zr oxides. In this respect, the conclusions of this review cannot be generalized to every type of oxide.

2. DENSITY FUNCTIONAL THEORY AND THE DESCRIPTION OF OXIDE SURFACES

DFT is the most widely used tool for the calculation of adsorption and reactions on solids surfaces, including oxides. A description of the foundations of DFT or of its various implementations is beyond the scopes of this review, and the reader is referred to more specialized publications.[23,24] Here I recall only some basic features and I introduce some of the more commonly used forms of exchange-correlations functionals that will be found in the course of the discussion on carboxylic acids adsorption and reaction on oxide surfaces.

Standard implementations of DFT are based on the Kohn−Sham equations[25] and on the use the local density or of the generalized gradient approximation (LDA and GGA, respectively) for the exchange-correlation functional. Various types of GGA functionals are available,[26] such as PW91,[27] PBE,[28] and RPBE.[29] It is well-known that LDA strongly overestimates bonds and adsorption energies, whereas GGA functionals are in much better agreement with experimental data.[30] Other problems are inherent to the use of LDA and GGAs, like for instance the underestimation of band gaps, the tendency to favor electron delocalization, and the accuracy of energy barriers for chemical reactions.

A practical way to improve the description has been proposed about 20 years ago by Becke who suggested to use a portion of the exact Fock exchange in the exchange functional in order to minimize the self-interaction error.[31] This is the first example of the so-called hybrid functionals, and the functional is known as B3LYP, where B stays for Becke exchange functional, LYP for the correlation functional of Lee, Yang and Parr,[32] and 3 is the number of parameters fitted to reproduce the thermochemistry of a given set of molecules. This approach turned out to be very successful and became rapidly of common use in the quantum chemistry community. One should notice that very similar results are obtained when the Becke exchange is combined with other correlation parts, as in the B3PW functional.[33] Hybrid functionals have then been expanded and formulated on a more solid ground. This is the case of the PBE0[34−36] and most recently, HSE[37−39] functionals. The application of hybrid functionals to periodic systems has been restricted for about a decade to codes based on Gaussian basis sets like the CRYSTAL code.[40] In recent years, also the community of solid state physicists started to use hybrid functionals after these have been implemented in plane wave codes.[41−44] However, the computational effort to evaluate the Fock exchange under periodic boundary conditions using plane waves is about 2 orders of magnitude that required for a normal GGA calculation, still limiting the use of this approach.

A more pragmatic approach to describe transition metal or rare-earth oxides is the so-called DFT+U approach. These systems contain electrons in partially filled d or f states, which are localized on particular metal atoms. In the spirit of the Hubbard model, Anisimov and co-workers[45] initially proposed it as an extension of the LDA approach. In practice, in these DFT(LDA/GGA)+U approaches one identifies a set of atomic-like orbitals that are treated with an orbital-dependent potential and an associated screened on-site Coulomb and

dx.doi.org/10.1021/cs500791w | ACS Catal. 2014, 4, 2874−2888

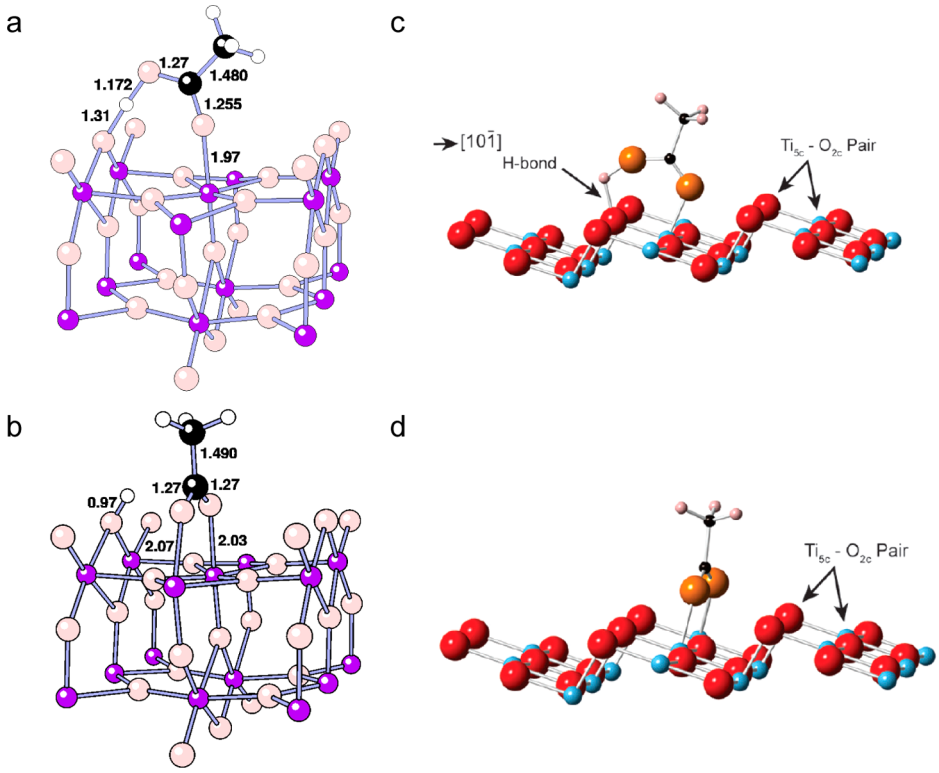

Figure 1. Some possible adsorption geometries of acetic acid on (a) TiO_2 rutile (110) surface, molecular monodentate structure; (b) TiO_2 rutile (110) surface, dissociative bidentate bridge structure. Violet (Ti), pink (O), black (C), and white (H). Distances in Å. Adapted from ref 55. (c) TiO_2 anatase (101) surface, molecular monodentate structure; (d) TiO_2 anatase (101) surface, dissociative bidentate bridge structure; (the position of dissociated H is not indicated; other structures, not shown, do also exist). Red (surface O); orange (acetate O); blue (Ti); black (C); pink (H). Adapted from ref 56.

exchange interaction parameters, U and J, respectively.[46] How to chose the atomic-like orbitals and effective U parameter ($U = U - J$) is a delicate issue. Recently, Hu and Metiu[47] have proposed that if one is interested in the redox properties of an oxide like TiO_2, the U parameter should not be chosen in order to properly reproduce the band gap (this procedure usually results in high values of the U term) but rather use U values that provide a good estimate for the energy of reduction of TiO_2 to Ti_2O_3. The use of DFT+U is an option only when the cost of running hybrid functional calculations is beyond the available computational resources.

Another important aspect, in particular for the study of molecules adsorbed on oxide surfaces, is that DFT/DFT+U with LDA or GGAs as well as hybrid-DFT do not properly account for van der Waals (vdW) dispersive interactions. In recent years, various approaches which account for vdW forces within the framework of DFT have been proposed (see ref 48 and references therein), and their use has considerably improved the description of molecular chemisorption.

A further step in the search of accurate functionals is represented by the M06-L functionals of Zhao and Truhlar,[49] which include not only density and its first derivative but also the kinetic energy density. Such functionals are called "meta-GGA" and have been shown to improve the description of thermochemistry and kinetics of reactions occurring on oxide surfaces.[50]

3. ADSORPTION OF CARBOXYLIC ACIDS ON TiO_2 AND ZrO_2

3.1. Titania Surfaces. In general, carboxylic acids adsorb strongly on metal oxides by splitting off of the acidic hydrogen and forming bonds between the carboxylate oxygen (or oxygens) and a cation (or two cations) of the oxide surface. This strong bond makes carboxylates ideal linker molecules to connect organic functional groups to oxide surfaces. This approach is widely used to prepare self-assembled monolayers on metal oxides,[51] to link visible light-absorbing dyes to titania for dye-sensitized solar cells,[52] or to bind organic units to inorganic oxide clusters to form three-dimensional organic−inorganic frameworks.[53]

There is general consensus from first-principles calculations that acetic acid adsorbs dissociatively on the rutile TiO_2(110) surface;[54,55] on the contrary, there is conflicting experimental and theoretical evidence for the adsorption of carboxylic acids on the (101) surface of anatase.[56−58] Recent studies suggest a higher stability of the monodentate associative mode for anatase TiO_2.[59−62] The bonding modes of acetic acid on the surface of rutile TiO_2(110) are shown in Figure 1; the oxygen atoms of the carboxyl group bind to the surface Ti atoms in either monodentate or bidentate mode[55] (these results refer to calculations performed at the PW91 level with the CASTEP program[63]). The molecular dissociated acid adsorbed in bridge mode is bound by 31.2 kcal/mol; the molecularly bound monodentate complex is only about 2 kcal/mol less stable.[55] This result alone shows the existence of competing adsorption modes on the titania surface. Further

dx.doi.org/10.1021/cs500791w | ACS Catal. 2014, 4, 2874−2888

data on the adsorption of carboxylic acids on titania can be found in some relevant reviews.[64−66]

Two of the several possible configurations of acetic acid on the (101) anatase surface are shown in Figure 1;[56] the carboxyl group can bind to the surface Ti atoms in either a monodentate or a bidentate mode.[55] Notice that a structure rotated by 180° was found to be more stable than that shown in Figure 1.[68] Recent work suggests a new binding mode of acetic acid characterized by proton insertion below the first layer of oxygen atoms.[60] Theoretical modeling of formic acid on the anatase (101) surface presents conflicting pictures regarding the predicted stability of the various conformations. Some calculations suggest that molecular monodentate is the most stable arrangement,[67,68] whereas others predict a bidentate arrangement.[69] Given the similar adsorption energies found for mono- and bidentate acetic acid on the rutile TiO_2(110) surface, this is not surprising. An important factor in determining the stability of the bidentate structure on TiO_2 surfaces is the increased separation of the Ti_{5c} sites on anatase (101) (3.78 Å) relative to rutile (110) (2.96 Å), which could result in an increased strain of the bond. Still, a recent room temperature STM study of acetic acid adsorption on the anatase (101) surface concluded that the most likely binding geometry is that of dissociative bidentate between two Ti_{5c} sites in the [010] direction.[56] The low mobility of the acetate at 300 K is comparable with that for the bidentate binding of carboxylates on rutile TiO_2(110) and supports the view of a relatively strong interaction with the anatase TiO_2(101) surface.

Thus, one can conclude that there is evidence for a similar binding mode of acetic acid on the most stable surfaces of rutile and anatase TiO_2. However, although there is consensus on the formation of a dissociatively adsorbed bidentatate carboxylate on rutile, this is still debated for anatase.

So far, only DFT calculations on the interaction of gas-phase molecules with the solid oxide surface have been presented. Recently, papers that overcome this DFT approximation have been released by including the effect of the solvent.[60−62] The presence of the solvent influences the molecule adsorption modes[61] as well as the activation energy for adsorption/desorption.[59] This is relevant because different adsorption modes can influence the overall reactivity of the system.

However, one has to mention that experimental evidence for the existence of monodentate carboxylic acids adsorbed on TiO_2 has also been reported. Pei and Ponec[70] examined adsorption and reaction of acetic acid on TiO_2 using FT-IR and showed that upon heating to 373−573 K, the IR band corresponding to the monodentate species gradually disappeared leaving only the bands associated with strongly bound bidentate carboxylates. Because only bidentate carboxylates can be observed at 573 K, the typical temperature at which ketonization starts to occur, they suggested that bidentate carboxylates are the species of crucial importance in the catalytic process.[70]

However, contrary to ref 70, Kim and Barteau[16] using TPD found that in order to generate ketone two acetate species involved in bimolecular ketonization should be coordinated in a monodentate mode to the same Ti on the {114}-faceted rutile (100) surface[71] (Figure 2, see reaction 5). In particular, they suggested that the reaction involves the 4-fold coordinated Ti^{4+} cations, which are present only on the {114}-faceted surface, and that these Ti^{4+} cations are the

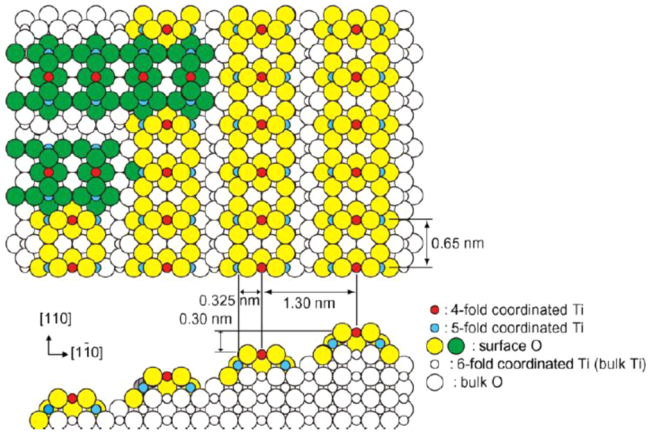

Figure 2. Top and side views of the stoichiometric model for the {114}-faceted TiO_2(100) surface which shows the 4-fold coordinated Ti atoms that are supposed to bind two carboxylate molecules. Small and large circles represent Ti and O atoms, respectively. Reproduced with permission from ref 71. Copyright 2008 Elsevier.

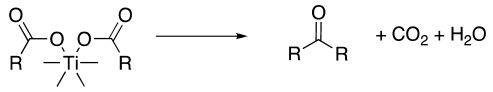

(5)

active sites for the ketonization because their multiple coordination vacancies allow them to accommodate bonding of the two carboxylate intermediates required for this bimolecular reaction. So far this idea has not found direct support from DFT calculations.

Thus, according to the literature, different adsorption modes are possible for carboxylate species involved in ketonization reactions. Switching from one form to another can be important to determine the most favorable mechanism for the reaction and the nature of the transition state formed.

3.2. Zirconia Surfaces. More limited is the number of studies on the adsorption of carboxylic acids on the surface of ZrO_2.[72,73] ZrO_2 can exist in at least five polymorphs.[74,75] At room temperature, only the monoclinic structure is stable. Around 1480 K, monoclinic zirconia undergoes a transition to a tetragonal phase, further converted at 2650 K into the cubic fluorite phase.[76] The most stable monoclinic polymorph has limited practical applications because of the crumbling of the ceramic components commonly observed during cooling from the tetragonal phase.[77] On the contrary, the high-temperature polymorphs (tetragonal and cubic) exhibit excellent mechanical, thermal, chemical, and dielectric properties.[78] The room-temperature stabilization of high-symmetry polymorphs of ZrO_2 is commonly achieved either by transition metal doping or by preparation of nanocrystalline phases.

All the calculations reported so far on the adsorption and reactivity of carboxylic acids on zirconia have been done on the monoclinic phase, which is stable at room temperature. However, it has been observed that doping zirconia with alkali metals results in an improved activity in the ketonization reaction, and this has been attributed to the stabilization of the tetragonal phase.[79] This suggests that DFT studies on the tetragonal phase can also be of interest.

Also on ZrO_2, the carboxylates bind to Lewis acid sites of the surface either in monodentate or bidentate configurations; these latter are generally more stable. It has been proposed that in the bidentate configuration the bonding can involve

dx.doi.org/10.1021/cs500791w | ACS Catal. 2014, 4, 2874−2888

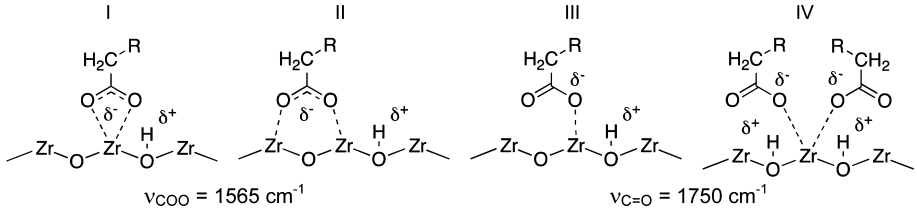

Figure 3. Interaction modes of a carboxylic acid with Lewis acid sites of the zirconia surface. Adapted from ref 73.

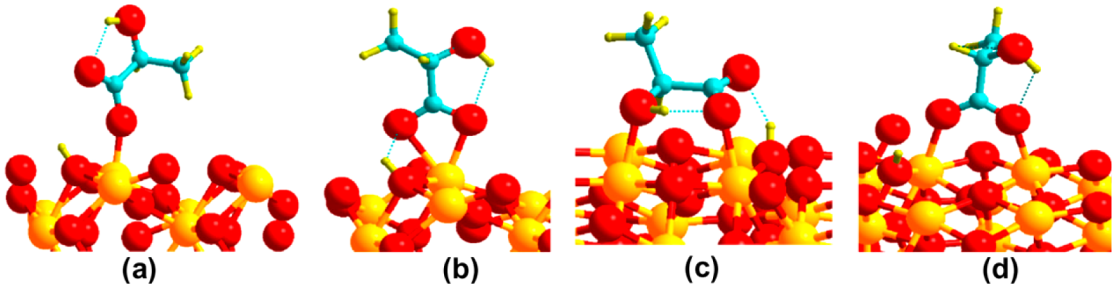

Figure 4. Most favorable structures of lactic acid adsorbed on the (011) surface of monoclinic ZrO_2. (a) monodentate mode with O−H dissociation (structure III in Figure 3, E_{ads} = 42.9 kcal/mol). (b) Bidentate chelating with O−H dissociation (structure I in Figure 3, E_{ads} = 39.4 kcal/mol). (c) Bidentate bridging mode with O−H dissociation (E_{ads} = 53.3 kcal/mol). (d) bidentate bridging mode with O−H dissociation (structure II in Figure 3, E_{ads} = 62.3 kcal/mol). Reproduced with permission from ref 82. Copyright 2013 Elsevier.

one or two surface cations giving a chelating bidentate complex (I) or a bridging bidentate configuration (II), as depicted in Figure 3. A distinction of the two species can be based on IR spectroscopy.

Periodic DFT calculations using the VASP code[80,81] and the PBE functional have been performed on the adsorption of lactic acid ($CH_3CH(OH)COOH$) on various faces of monoclinic ZrO_2 by Hammaecher and Paul.[82] Lactic acid presents three available atoms for adsorption on m-ZrO_2, the two oxygen atoms of the carboxyl group and the oxygen atom of the alcohol group. This leads to several possible binding modes and to a wide range of possibilities for dissociative adsorption and further reactivity. It is of some help for the modeling of these systems the fact that the preferred adsorption sites for lactic acid on ZrO_2 are the same as for water.[82] The estimated adsorption energies of lactic acid carboxylate species (I), chelating bidentate,[82] are 39.5 kcal/mol on ZrO_2(011), 38.2 kcal/mol on ZrO_2(101), and 12.9 kcal/mol on ZrO_2(111); carboxylate species (II), bidentate, is bound by 62.2 kcal/mol on ZrO_2(011), 55.5 kcal/mol on ZrO_2(101), and 36.4 kcal/mol on ZrO_2(111), respectively.[82] It is clear that interaction with two surface Zr cations is always largely preferred and that the open (011) and (101) surfaces bind more strongly.

Still, also on ZrO_2 formation of monodentate carboxylates, see structures III and IV in Figure 3, has also been suggested.[5] An absorption band at 1750 cm^{-1} corresponds to the stretching vibrations of carbonyl groups of these carboxylates. For instance, acetic acid chemisorption on MgO−SiO_2 leads to monodentate acetate with an absorption band at 1747 cm^{-1}.[83] As mentioned above, the existence of bimolecular monodentate species on oxide surfaces, like structure IV in Figure 3, has been long considered to be quite relevant for the mechanism of ketonization reactions (see the discussion below).[16]

DFT calculations on monomolecular monodentate adsorption of lactic acid over ZrO_2 demonstrated the possible formation of configuration (III), Figure 3.[82] The computed adsorption energies of lactates in this configuration depend strongly on the surface chosen: 42.8 kcal/mol on ZrO_2(011), 40.0 kcal/mol on ZrO_2(101), and 22.5 kcal/mol on ZrO_2(111).[82] In all cases, the monodentate structure (III) is less stable than the bidentate bridging form (II). Some of the optimal structures of lactic acid adsorbed on the (011) surface of monoclinic ZrO_2 are shown in Figure 4.

In general, adsorption on Zr ions with lower coordination leads to stronger adsorption energies. The general trend for the lactic acid adsorption mode on (011), (101), and (111) monoclinic zirconia surfaces is that the bidentate bridging one with OH bond dissociation is preferred (two variants of this bonding mode have been found).[82] These two modes of interaction of lactic acid with zirconia are almost equally probable, and could potentially lead to different reactions pathways, an effect that may limit a good control of the selectivity on these surfaces.

The adsorption of acetic, propionic (CH_3CH_2COOH), and isobutyric ($(CH_3)_2C(OH)COOH$) acids on the most stable ($\bar{1}11$), (111), and ($\bar{1}01$) surfaces of monoclinic ZrO_2 has been studied by Ignetchenko[72] using a periodic DFT approach at the GGA level (PW91 functional[27]) and the DMol3 software.[84] He found that the relative strength of the various adsorption sites is the same for acids with different chain length. Adsorption of carboxylic acids on zirconia closely resembles that found on rutile (110), (011), and anatase (001) surfaces. In particular, a preference for dissociative over molecular adsorption has been found on all zirconia surfaces studied. The structure of acetic acid adsorbed on the (111) surface of monoclinic ZrO_2 is shown in Figure 5. Here the acetate fragment is bound in a bidentate bridging mode over two surface Zr^{4+} cations with an adsorption energy of about 44 kcal/mol. Notice that this adsorption energy is about 12 kcal/mol higher than that obtained for the same bonding configuration and the same functional on TiO_2(110).[55]

In the same study,[72] it has been found that the arrangement of two carboxylic acids on the same Zr atom (structure IV in Figure 3) is highly unfavorable. Despite the fact that a Zr

dx.doi.org/10.1021/cs500791w | ACS Catal. 2014, 4, 2874−2888

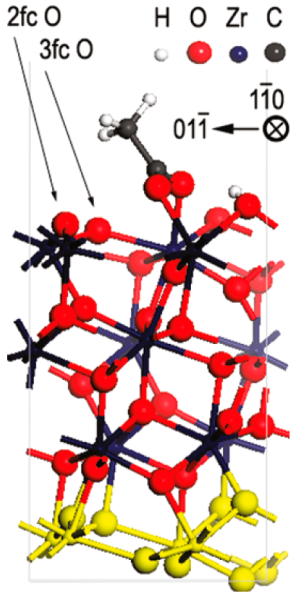

Figure 5. Acetic acid adsorption on the (111) surface of monoclinic zirconia with H dissociation; acetate adsorbed in bidentate bridging mode; H moves to the O_{2c} lattice ion. Reproduced with permission from ref 72. Copyright 2011 American Chemical Society.

atom with a double coordinative unsaturation has been considered, a significant steric repulsion between two alkyl groups results in an energy increase. This seems to contrast with the widely accepted concept of the adsorption of two carboxylic acids on the same coordinatively unsaturated metal atom in the ketonization mechanism.[16] In view of these recent computational results, this concept may need to be reconsidered in a more critical way.

4. REACTIONS OF CARBOXYLIC ACIDS ON TiO_2 AND ZrO_2

4.1. Benchmark Calculations: Gas-Phase Reactivity. The complexity of the reactions involved in ketonization processes is such that at the moment gas-phase reactivity can be explored in more detail than the reactivity of carboxylic acids on the surface of a solid catalyst. Also from the point of view of the accuracy of the calculations, gas-phase molecular reactions can be studied at an higher level of theory than reactions involving gas/solid or liquid/solid interfaces.

Very recently, an extensive quantum mechanical study has been reported to compare activation energies and rate constants for unimolecular decomposition pathways of saturated and unsaturated carboxylic acids that are important in the production of biofuels or as intermediates in the synthesis of biofuels.[85] The work was done using the Gaussian09 suite of programs[86] and the M06-2X hybrid meta-GGA functional of Truhlar and Zhao[87] with an extended basis set. Decarboxylation and dehydration reactions 1−3 were considered, and the energies and structures of all species were calculated and fully optimized. A robust systematic search technique was used to optimize all reactant and product conformations.[88] The performance of the computational methods adopted was benchmarked against two well-known chemical decomposition reactions, the dehydration of ethanol and the decomposition of ethyl acetate. The computed activation energies were found to be within 1.5 kcal/mol of the experimental values; the Arrhenius pre-exponential factors were within a factor of 5 from experiment,[85] which can be considered as a very good result. This shows what can be done nowadays in terms of chemical accuracy in the calculation of activation barriers and reaction mechanisms for gas-phase reactions involving nontransition elements.

The competition between decarboxylation and dehydration was studied for a series of saturated and unsaturated organic acids with 2−4 carbon atoms.[85] The enthalpy of reaction (ΔH) for acetic acid decarboxylation, reaction 1, is negative (exothermic), whereas those for dehydration, reactions 2 and 3, are positive (endothermic) (see section 1). Quite challenging is the calculation of activation barriers. The experimental activation energies for the competing decarboxylation and dehydration pathways at about 1000 K have been determined some time ago and are 62.0 and 67.5 kcal/mol, respectively.[89] Theoretical calculations based on the CASSCF approach reported activation energies of 71.8 kcal/mol for reaction 1, 76.4 kcal/mol for reaction 2, and 73.1 kcal/mol for reaction 3, respectively,[90] in good agreement with the experimental estimates. These values are essentially reproduced by the DFT approach of Clark et al.[85] They thus considered competing decomposition pathways for a family of possible saturated and unsaturated C2−C4 acids in order to estimate branching ratios between the decarboxylation and dehydration pathways. The activation energies and predicted kinetic values for acids of importance to biofuels were also calculated and are summarized in Figure 6.

The computed barrier heights to decarboxylation and dehydration are similar for saturated acids (about 71 kcal/mol). α,β-Unsaturation lowers the barrier to decarboxylation by about 2 kcal/mol while increasing the barriers to dehydration by about 3 kcal/mol. β,γ-Unsaturation results in a small lowering in the barrier height to decarboxylation (which became about 70.0 kcal/mol) as well as in the dehydration pathway (reduction from 2 to 5 kcal/mol). In general, the activation barriers for decarboxylation and dehydration do not seem to change much for different carboxylic acids.

As mentioned above, the work of Clark et al.[85] represents probably the most complete theoretical study to predict kinetic values for acids of importance in biofuels production. It should be mentioned, however, that this kind of accuracy is difficult to achieve for chemical reactions occurring on solid surfaces.

4.2. Enolization on ZrO_2. While several studies exist on the adsorption of carboxylic acids on the surface of TiO_2 and ZrO_2 (see section section 3), the number of DFT studies on the reactivity of the adsorbed species is rather scarce. This is not surprising due to the large number of possible reaction paths that are involved, as discussed above. Once a carboxylic acid is adsorbed on an oxide surface, one of the possible reactions is the enolization, i.e. the abstraction of an α-hydrogen by the basic sites of the surface, Figure 7. Experimental evidence for the enolization of surface carboxylates comes from the observation of their α proton exchange for deuterium.[91] The enolized form of carboxylate, $R_2C{=}COO^-$, resembles the structure of the so-called "surface ketene" proposed as one of the possible intermediates in the mechanism of carboxylic acid ketonization.[12,15] Ignatchenko has studied the enolizaton reaction of carboxylic acids on three surfaces of monoclinic zirconia by means of DFT

dx.doi.org/10.1021/cs500791w | ACS Catal. 2014, 4, 2874−2888

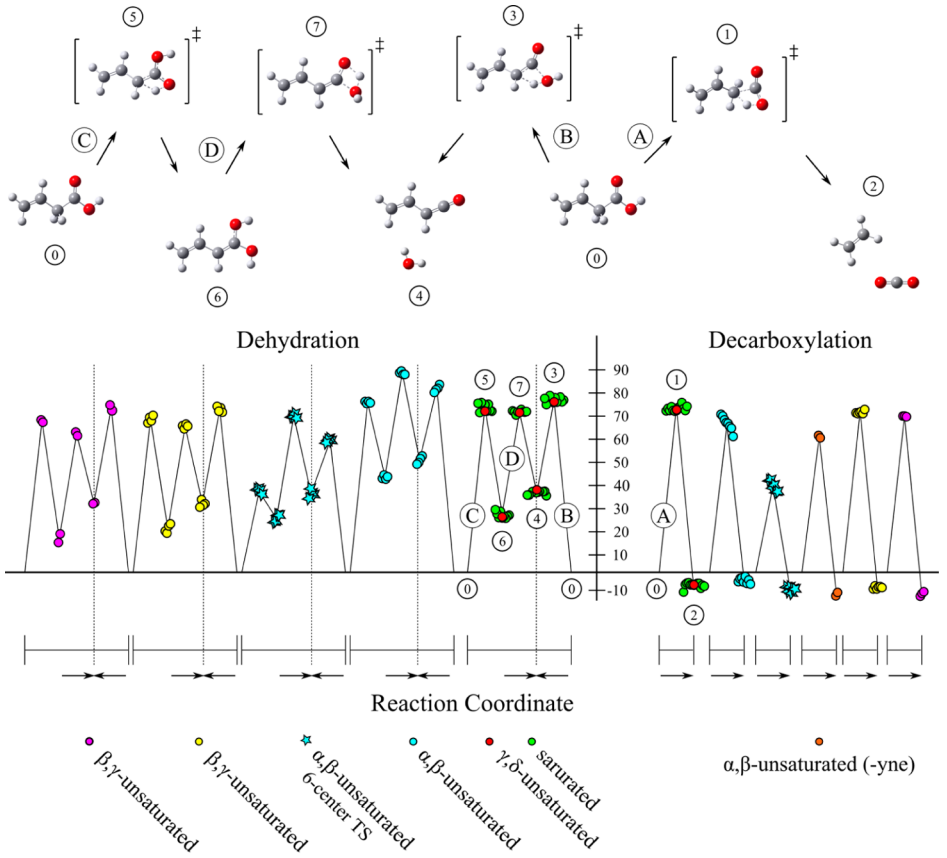

Figure 6. Potential energy diagram for the decarboxylation (right of vertical axis, A) and dehydration (left of vertical axis, B–D) of some organic acids. For the dehydration pathways, the concerted mechanism lies to the right of the dotted line, whereas the stepwise mechanism lies to the left. The units of the vertical axis are in kcal/mol. The energies represent the difference between the reactant and transition state. Each set of different colored circles represents a separate class of organic acid (e.g., green represents saturated acids). The lettered circles denote reaction pathways. The numbered circles represent the following: 0: starting acid; 1: decarboxylation transition state; 2: decarboxylation products; 3: dehydration transition state; 4: dehydration products; 5:1,1-enediol formation transition state; 6:1,1-enediol intermediate; 7:1,1-enediol dehydration transition state. A cartoon representation of the competing pathways is illustrated, using crotonic acid, at the top of the figure. Reproduced with permission from ref 85. Copyright 2014 American Chemical Society.

calculations,[72] using the PW91 functional[27] and the DMol3 code,[84] Figure 7.

First of all, the carboxylic acid adsorbed on the surface dissociates with formation of a bidentate bridging carboxylate and an OH group. Then, a lattice oxygen of the ZrO_2 surface can readily abstract the hydrogen atom in the α position to the carboxylic group, Figure 7. Acetic, propionic, and isobutyric acids exhibit similar reaction barriers for enolization, in the range 25–33 kcal/mol, depending on the specific zirconia surface.[72] All studied deprotonation reactions exhibit a late transition state where the α carbon has a nearly sp^2 geometry. The geometry of the developing double bond center in the enolization reaction becomes increasingly flat as the reaction progresses from the starting carboxylate to the transition state and further to the enolized product.

In summary, the work of Ignatchenko has shown that enolization of carboxylic acids occurs on monoclinic zirconia surfaces with a relatively low activation energy barrier, which is basically independent of acid branching. The 2-fold coordinated lattice oxygen on the most stable surface of m-ZrO_2 is the preferred basic site for hydrogen abstraction and enolization of adsorbed carboxylates.

4.3. Ketonization on ZrO_2. Due to the complexity of the chemical process, ketonization reaction mechanisms on oxide surfaces have not been discussed based on DFT calculations until very recently. In 2013 Pulido et al. reported an extensive and detailed study on the intermolecular ketonic decarboxylation of monocarboxylic acids catalyzed by metal oxides.[92] The reaction mechanism of acetone formation over monoclinic zirconia was investigated by means of periodic DFT calculations (PW91 functional, VASP code;[80,81] dispersion interactions have been included by means of the D3 method[93]). As discussed above, some controversy exists about the reaction mechanism that takes place during ketonic decarboxylation. The classical and widely accepted mechanism is the already mentioned formation of a β-keto acid intermediate from the abstraction of an α-hydrogen atom (see section 1).[8] The performance of alumina, silica, ceria, zirconia, and mixed zirconium cerium oxides, in the decarboxylation of decanoic acid into 10-nonadecanone was first investigated experimentally.[92] It was concluded that monoclinic ZrO_2 is a suitable catalyst for the ketonic decarboxylation of carboxylic acids with a wide range of molecular weights, from acetic acid to fatty acids. To

dx.doi.org/10.1021/cs500791w | ACS Catal. 2014, 4, 2874–2888

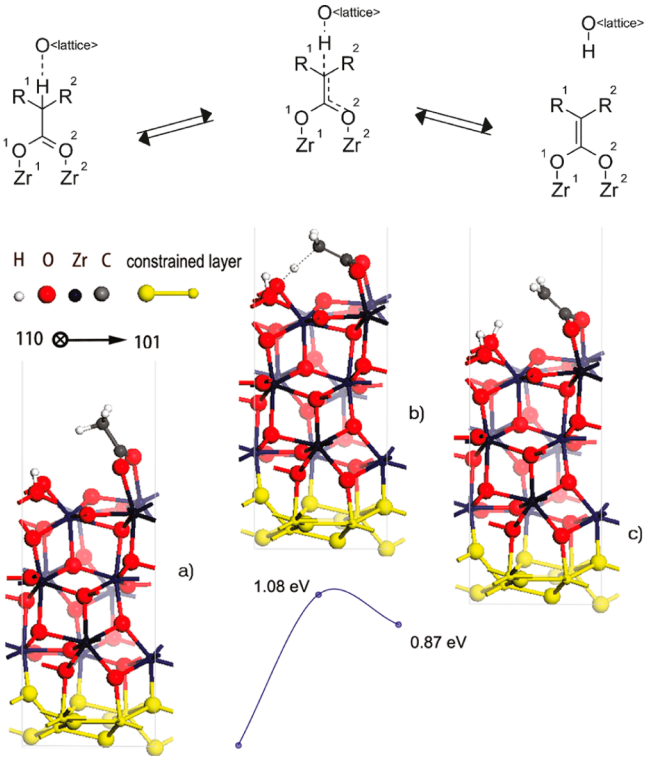

Figure 7. Enolization of acetate on the (111) surface of monoclinic zirconia. Top: schematic view of the reaction mechanism; bottom: structure of the reactants and intermediates: (a) Acetate adsorption in bidentate bridging mode; the dissociated H is attached to the O_{2c} lattice ion; (b) Optimized transition state; (c) Enolized acetate. Reproduced with permission from ref 72. Copyright 2011 American Chemical Society.

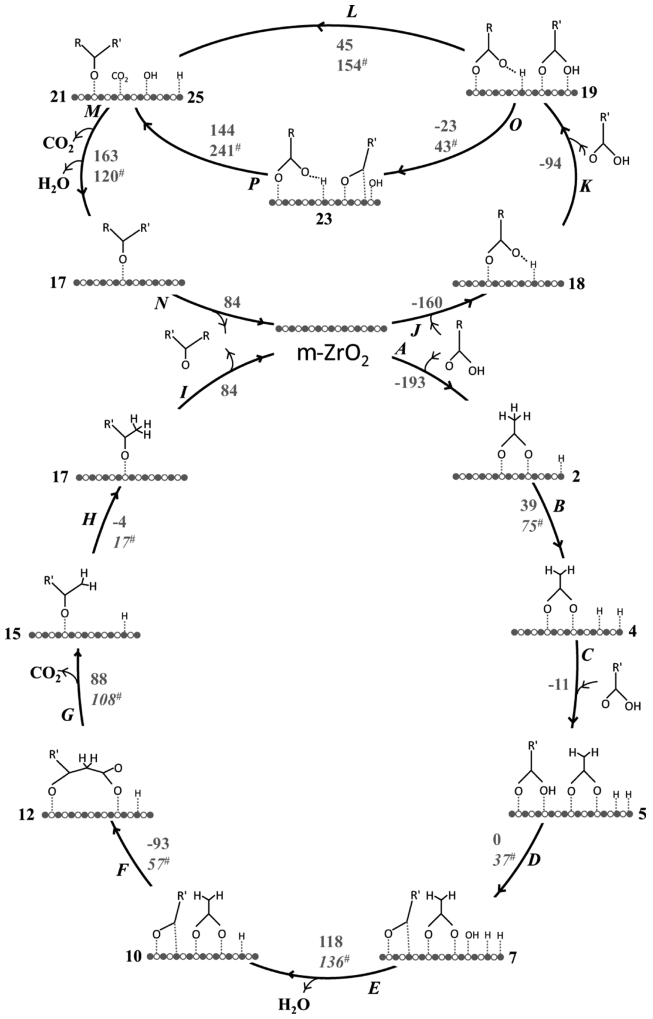

Figure 8. Reaction pathways for ketonic decarboxylation of acetic acid (R=R′=CH_3) over m-ZrO_2 following the β-keto acid (bottom) and concerted (top) routes. PW91-D3 reaction and activation (in italic and with superscript #) energies (in kJ/mol) of each step are shown. Zr and O atoms of the ZrO_2 surface are represented by empty (o) or filled (•) dots, respectively. For the sake of clarity, double bonds and charges are not shown. Reproduced with permission from ref 92. Copyright 2013 Wiley-VCH.

understand the ketonic decarboxylation reaction mechanism at the molecular scale, the formation of acetone, CO_2, and H_2O from the decarboxylation of two molecules of acetic acid was investigated at the DFT level on the (111) surface of m-ZrO_2, see Figure 8. An impressive number of calculations was performed to understand this reaction mechanism as well as other competitive reaction routes, providing in this way a general description from a DFT point of view of the ketonic decarboxylation reaction mechanism on m-ZrO_2.[92]

Several adsorption modes of acetic acid are possible on the surface of m-ZrO_2, with interaction energies between −16.0 and −41.1 kcal/mol, in agreement with other studies on this system.[72] The complex reaction scheme that follows acetic acid adsorption is shown in Figure 8. The pathway A → B → C → D → E → F → G → H → I shows schematically ketonic decarboxylation taking place along the β-keto acid route as computed by DFT. The process starts with the formation of the most stable acetic acid adsorption complex with release of 46.2 kcal/mol (193 kJ/mol) and formation of an acetate intermediate (barrierless). Then, abstraction of a α-hydrogen atom by the surface O_{2c} atom leads to the formation of an acetic acid dianion intermediate (step B in Figure 8) with an endothermic step (ΔE = 9.3 kcal/mol or 39 kJ/mol) and an activation barrier of 17.9 kcal/mol (75 kJ/mol). The reaction continues with adsorption of a second molecule of acetic acid near the previously formed dianion (step C in Figure 8). It appears that the vicinity of a previously dissociated species favors an associative adsorption of the second molecule, an aspect that is not discussed in ref 92. The second molecule of acetic acid can be easily dehydroxylated, leading to the formation of an adsorbed acylium intermediate (step D in Figure 8). At this point, both a hydrogen and hydroxyl groups have already been removed from the acetic acid molecules and can be combined to form a water molecule (step E in Figure 8). After H_2O desorption, an acetic acid dianion and an acylium intermediate are adsorbed on the ZrO_2 surface on vicinal positions. Here, the terminal CH_2 carbon atom of the dianion attacks the carbon atom of the carbonyl group of the acylium intermediate (step F in Figure 8), leading to the formation of the β-keto acid intermediate. This step is exothermic by 22.2 kcal/mol (93 kJ/mol) and implies an energy barrier of 13.6 kcal/mol (57 kJ/mol). Next, acetone enolate and CO_2 can be formed from the β-keto carboxylate intermediate (step G in Figure 8) by breaking of the C−C bond with an endothermic step by 21.0 kcal/mol (88 kJ/mol) and an activation barrier of 25.8 kcal/mol (108 kJ/mol). It is concluded that this is also the rate-determining step of the entire β-keto acid route. This result,

dx.doi.org/10.1021/cs500791w | ACS Catal. 2014, 4, 2874−2888

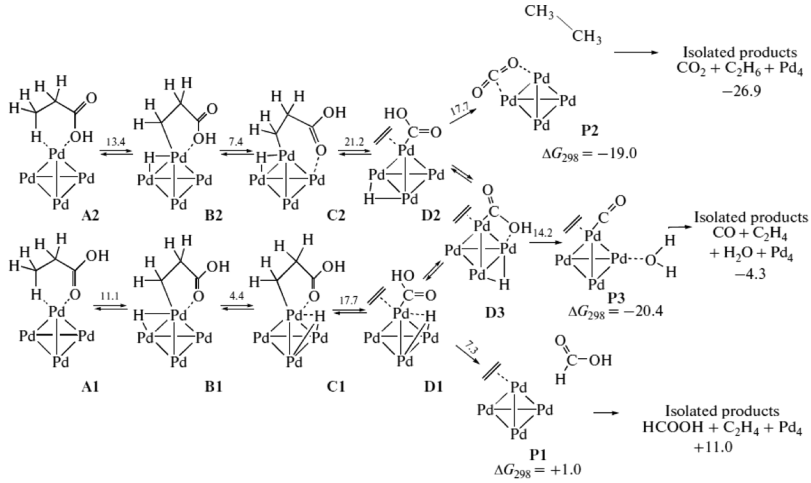

Figure 9. Schematic representation of the reactions of transformation of propionic acid over a Pd_4 unsupported catalyst. Reproduced with permission from ref 94. Copyright 2011 Springer.

however, is a bit surprising since it is usually accepted that the decomposition of the β-keto carboxylate intermediate is rapid and easy. Indeed, these intermediates have never been observed due to their rapid evolution. The next step (step H in Figure 8) consists in the transfer of an adsorbed H atom to the acetone enolate intermediate, with a nearly thermoneutral process and a low barrier of 4.1 kcal/mol (17 kJ/mol). The catalytic cycle is closed by acetone desorption, an endothermic step by 20.1 kcal/mol (84 kJ/mol, see step I in Figure 8).

Figure 8 also shows another possible reaction path (see steps J → K → L → M → N) called concerted reaction route and an alternative mechanism (steps O → P in Figure 8). The calculations show that in both cases the barriers involved are higher than for the mechanism based on β-keto acid intermediates discussed above. Thus, the DFT calculations suggest that ketonic decarboxylation of monocarboxylic acids and the formation of ketones proceeds predominantly by means of the β-keto acid mechanism. This theoretical result is supported also by other experimental evidence.[92] Notice that this reaction path does not imply the adsorption of two carboxylic acids on the same low-coordinated Zr ion, structure IV in Figure 3, but rather on two different Zr ions in neighboring positions. Furthermore, the mechanism has been investigated for a regular surface plane of m-ZrO_2, thus neglecting the possible role of low-coordinated ions of the surface in the reaction.

It is interesting to comment at this point on the role of dispersion forces for the reactivity described above. The reaction pathways for acetic acid decarboxylation have been obtained also at the PW91 level, i.e. without inclusion of dispersion, and the results can thus be compared to the PW91-D3 data reported above. The inclusion of intermolecular dispersion interaction does not change the energy profile obtained at the PW91 level. The differences between calculated PW91 and PW91-D3 activation barriers are at most 4 kcal/mol, suggesting a minor role of dispersive interactions, at least for this specific case.[92]

5. REACTIONS OF CARBOXYLIC ACIDS ON METAL CLUSTERS SUPPORTED ON OXIDE SURFACES

5.1. Unsupported Metal Clusters. The conversion of fatty acids into fuels and chemical intermediates requires catalytic deoxygenation, which is often carried out over supported Pd metal particles. The formation of CO or CO_2 implies the cleavage of the C−C bond in R-COOH. This problem has been studied experimentally for the transformation of stearic acid ($CH_3(CH_2)_{16}COOH$) on Pd/Al_2O_3 catalysts, and the results have been complemented by quantum chemical calculations.[94] Here I concentrate on this aspect. The real system was modeled by using a molecule of propionic acid as reactant and an unsupported Pd_4 cluster to represent the supported metal particle. Since gas-phase Pd_4 has a tetrahedral shape, this is the geometry adopted for the Pd nanocluster. The calculations where done at the DFT level using the PBE exchange-correlation functional[28] and the Priroda code.[95,96]

The use of a gas-phase metal cluster to mimic the behavior of a supported Pd nanoparticle is not uncommon in computational studies, and is based on the assumption that the oxide support has no role in the reactivity ("inert support"). While this may be true in general, it is no longer true when the supported metal unit is very small. In this case, in fact, the electron exchange at the interface between the metal and the oxide support can significantly alter the chemical properties of the metal particle and can result in a completely different chemical reactivity.[97,98] In this case some care is necessary when comparison with experiment is done.

The results of the computational work by Berenblyum et al.[94] are summarized in Figure 9 which schematically reports the reactions of transformation of propionic acid over a palladium catalyst. The reaction starts with the adsorption of the reacting acid molecule on the Pd_4 cluster with the coordination to a Pd atom and the simultaneous interaction of one of the two oxygen atoms of RCOOH and the hydrogen atom at the β-carbon (see A1 and A2 in Figure 9). Pd atoms are known to insert into C−H bonds; when this occurs the intermediates B1 and B2 can form, Figure 9. This can be followed by H migration, C1 or C2, followed by C−C bond scission and formation of adsorbed etylene (D1 or D2) and further desorption of HCCOH (P1), CO+H_2O (P2), or CO_2 (P3). The calculations show that the rate-limiting step of the reaction is the cleavage of C−C bond in the acid molecule. From these calculations it was concluded that although the decarboxylation reaction is the most favorable in terms of thermodynamics, it is likely that kinetic reasons make

dx.doi.org/10.1021/cs500791w | ACS Catal. 2014, 4, 2874−2888

decarbonylation dominate during the conversion of acid molecules in the coordination sphere of Pd.[94]

5.2. Supported Metal Clusters. Recently, it has been found that Au nanoparticles supported on TiO_2 are highly selective in activating the C−H bonds at the C2 and C3 positions for linear organic acids (propionic and butyric acid) to form unsaturated carboxylate surface intermediates.[99] Using infrared spectroscopy (IR) and DFT calculations, unsaturated acrylate (CH_2=$CHCOO^-$) and crotonate (CH_3CH=$CHCOO^-$) were observed to form from propionic acid and butyric acid ($CH_3CH_2CH_2COOH$), respectively, on a catalyst with about 3 nm diameter Au particles on TiO_2 at 400 K. The high selectivity of Au/TiO_2 suggests that the sites and mechanisms for the activation of organic acids are different from those active on supported Pd or Pt nanoparticles.

The mechanism of the reaction has been investigated with the help of DFT calculations performed at the DFT+U level using the code VASP[80,81] and the PW91 functional.[27] In particular, calculations were carried out to examine the mechanism of acrylate formation and to determine the frequencies for adsorbed acrylate and crotonate species in order to compare them with IR spectroscopic results. The TiO_2 support was simulated by using a rutile TiO_2(110) supercell. The 3 nm Au particles supported on TiO_2 were simulated by a closely packed Au nanorod model anchored to the TiO_2 (110) support.[99]

The experiments and the DFT simulations provide evidence that propionate ($CH_3CH_2COO^-$) dehydrogenates to acrylate (CH_2=$CHCOO^-$) under oxidation conditions. Similarly, butyrate is found to convert into crotonate upon oxidative-dehydrogenation on Au/TiO_2. The calculated potential energy profile for the formation of acrylate from propionic acid is reported in Figure 10.

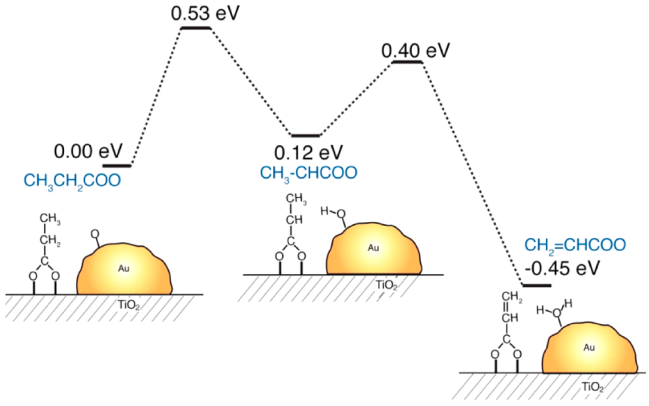

Figure 10. Calculated potential energy diagram for the oxidative dehydrogenation of propionate at the Au/TiO_2 interface to form an acrylate surface intermediate. Reproduced with permission from ref 99. Copyright 2014 American Chemical Society.

First, the O−H bond of propionic acid is readily cleaved by the bridging O_{2c} sites on the TiO_2 surface, resulting in the formation of surface propionate intermediates at the Au/TiO_2 interface (bidentate dissociative adsorption). Second, an O_2 molecule is activated at $Au-Ti^{4+}$ sites at the Au/TiO_2 interface and results in the formation of adsorbed atomic oxygen (O_{ad}) on the Au sites at the Au/TiO_2 perimeter. The resulting adsorbed atomic oxygen migrates on the Au particle and acts as a base that can effectively activate the C−H bonds involved in the oxidative dehydrogenation. In fact, a C−H bond at the C_α position can be activated by the basic O_{ad} species bound to Au with an activation barrier of 12.2 kcal/mol and formation of an adsorbed OH group on Au, Figure 10. This results in the formation of the CH_3CH−COO species. Then another H abstraction can occur from the OH group with formation of a water molecule adsorbed on Au and a acrylate adsorbed species (barrier 9.2 kcal/mol), Figure 10. The acrylate is 10.4 kcal/mol more stable than the original CH_3CH_2COO/Ti complex because of the formation of the C=C double bond and the reduction of the coadsorbed O atom to H_2O.[99]

The steps in the catalytic cycle involve activation barriers of about 7−12 kcal/mol, consistent with the moderate reaction temperatures (near 400 K) observed experimentally. Furthermore, the work points out the important role of the interface between the oxide surface and the supported metal particle in determining the chemistry of the process. This aspect has been suggested in several studies, mainly based on DFT calculations,[100,101] although direct unambiguous experimental evidence of the involvement of the metal/oxide perimeter of the supported nanoparticle is difficult to obtain.

6. KETONIZATION MECHANISMS AND THE ROLE OF SUPPORTED METALS

The above discussion clearly shows that, while ketonization of carboxylic acids has been known and studied for many years, the details of the reaction mechanism and the rate limiting steps are still under debate. Recent experimental studies by Pham et al.[102,103] on Ru/TiO_2 catalysts demonstrated that the ketonization rate is consistent with a bimolecular surface reaction mechanism indicating that two molecules of acetic acid are involved in the rate limiting step and the products compete for adsorption on the same type of sites. This contradicts other proposed mechanisms that consider monomolecular steps as rate limiting. For example, formation of a ketene intermediate or abstraction of an H_α atom has been previously proposed to be rate limiting.[104]

A bimolecular rate-limiting step is consistent with the following mechanisms: (a) direct concerted mechanism of two surface carboxylate species; (b) a surface carboxylate attacked by a ketene molecule; (c) a carboxylate (or acylium) attacked by an enolate species leading to the formation of a β-ketoacid

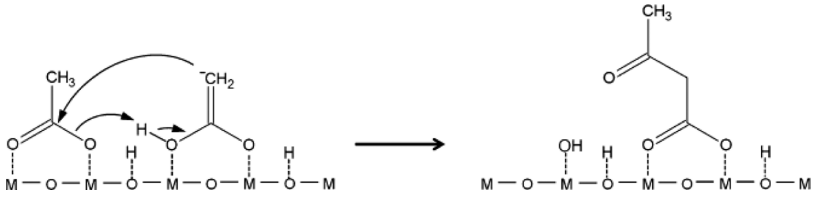

Figure 11. Proposed mechanism for β-keto acid formation step in ketonization reactions. Reproduced with permission from ref 102. Copyright 2014 Springer.

dx.doi.org/10.1021/cs500791w | ACS Catal. 2014, 4, 2874−2888

intermediate. As mentioned before, ketonization requires at least one α-hydrogen atom in the carboxylic acids that participate in the reaction for the formation of enolate species or ketene intermediates. This is consistent with mechanisms (b) and (c) but not with the direct concerted mechanism (a). Furthermore, the DFT study of Pulido et al.[92] discussed above has shown that the concerted mechanism (a) should be ruled out because of the high activation barrier and the preferred route via formation of a β-keto acid. At the moment, also thanks to the results of DFT calculations,[92] this seems the most plausible mechanism (see Figure 11).

The other points that need further discussion are the active sites involved in the reaction on the surface of TiO_2 or ZrO_2, the role of supported metals like Ru, and the redox properties of the oxide support. As mentioned in section 1, the nature of the active sites for ketonization has been discussed by Kim and Barteau[16] based on their study of ketonization on single crystal TiO_2. They ascribed the unique activity of the (114) surface to the presence of doubly unsaturated Ti cations. It has been suggested that prereduction, doping with other metals or deposition of metal particles can be a way to create defects and generate coordinatively unsaturated sites.[102] Furthermore, the catalytic activity of powder TiO_2 should increase by these modifications. For instance, the addition of Ru helps to enhance the reducibility of TiO_2 and this should result in the easier formation of coordinatively unsaturated Ti^{3+} sites. A similar effect has been found for ZrO_2 where the activity is enhanced by the presence of Zr^{3+} ions.[73,105]

Another important observation, which holds true for both TiO_2[102] and ZrO_2,[73] is that prereduction in H_2 significantly enhances the activity of the catalyst, whereas the activation energies and reaction orders remain unchanged. This leads to the conclusion that the prereduction treatment determines an increase of the active sites, without affecting the rate limiting step nor the intrinsic activity of the other active sites. By studying the EPR signal of Ti^{3+} species in nonreduced and prereduced $Ru/TiO_2/C$ catalysts, it has been found that a significant fraction of Ti^{3+} species can be formed upon the reduction treatment.[22] Although there is no doubt that reduction processes in TiO_2 and ZrO_2 lead to an increase of Ti^{3+} and Zr^{3+} ions,[106,107] and although it is possible that these species are preferentially located on the surface of the oxides, their role in the surface chemistry of carboxylic acids and in the ketonization process requires further studies at the atomistic level in order to be confirmed.

There is ample evidence in the literature that the Ti^{3+} and Zr^{3+} species correspond to localized electrons trapped in the 3d or 4d states of the transition metal atom (this is true at low temperature; at high temperatures, the electrons start to become mobile and delocalized). Still, the presence of unpaired electrons in the system, as proven by EPR measurements, can significantly alter the reactivity of the surface sites and can even result in a completely different mechanism for the surface reactions (as recently demonstrated for the case of formaldehyde polymerization over $(WO_3)_3$ clusters supported on TiO_2).[108] The role of the reduced Ti^{3+} and Zr^{3+} ions in ketonization reactions still needs to be investigated in detail and could lead to rather different reaction mechanisms.

7. CONCLUSIONS

Ketonization is a reaction which has been known in organic chemistry for a very long time. Still, the mechanisms that lead to the reaction of two carboxylic acids and to the formation of a ketone product are a matter of debate. Some firm points have been established thanks to the work done by several groups, like for instance the importance of the α-hydrogen abstraction, the need of pairs of Lewis basic and acid sites on the surface of the catalyst, or the role of low-coordinated cations. But many other points about the atomistic aspects of the reaction and the nature of the active sites remain to be understood. In the last 10−15 years, the advent of modern electronic structure theory approaches based on the density functional theory has provided additional pieces of information that turn out to be quite valuable to complement the experimental data.

In this respect, high quality calculations can be performed for reactions occurring in the gas-phase and both thermochemical values and activation barriers can be obtained from theory with a high level of accuracy. Calculations performed on the gas-phase reaction of carboxylic acids have clearly shown that different reaction paths are possible with similar activation barriers, an effect that can limit severely the selectivity of the process. This is also why reactions involving a solid catalyst are of great interest.

Modeling surfaces, and in particular transition metal oxide surfaces, is much more complex that modeling reactions that involve C−C, C−O, and C−H bond breaking and bond formation. The intrinsic nature of transition metal elements, their complex redox chemistry, the presence of localized electrons in d orbitals, and so forth are all elements that render the use of theory for the study of surface chemical reactions less straightforward. Intrinsic limitations in the present formulation of the exchange−correlation functionals used in DFT, like the well-known self-interaction problem, limit the accuracy of the computed thermodynamic and kinetic quantities. On top of this, one has to consider the complexity represented by the surface of an oxide, and the need to represent this complexity in the models used to study the reaction. Polycrystalline oxides used in catalysis exhibit different surface planes, each with a specific reactivity; they expose extended defects like steps, edges, dislocations, grain boundaries, where the reactivity can be very different from that of the regular surface planes; they contain significant amounts of point defects like impurity atoms, vacancies, hydroxyl groups, trapped electrons, among others, which vary considerably in type and number as a function of the preparation method and they present morphological irregularities. When prepared in nanostructured forms (ultrathin films, nanoparticles), oxides possess properties different from the bulk ones due to the low dimensionality of the system.[109]

So far, DFT calculations on adsorption and reactions involving carboxylic acids have been reported only for the most common regular surfaces of a few oxides. Among these, TiO_2 and ZrO_2 have been considered because of their importance as practical catalysts. Some very interesting results have been obtained on these systems, and some firm points start to emerge from these studies.

First of all, carboxylic acid dissociatively adsorb on the surfaces of rutile TiO_2 and zirconia forming a carboxylate unit and an OH group. The bridge bidentate structure where the carboxylate fragment interacts simultaneously with two surface Ti^{4+} or Zr^{4+} cations seems to be generally preferred, although in many cases, the monodentate binding mode is only slightly less stable. The situation is more complex for the (101) anatase surface. Several DFT reports indicate that the

dx.doi.org/10.1021/cs500791w | ACS Catal. 2014, 4, 2874−2888

monodentate associative mode is preferred and the question of the most stable adsorption mode remains open. Second, the presence of low-coordinated O ions on the surface can lead to the abstraction of an additional hydrogen atom from the C atom in α position with respect to the carboxyl group. This reaction, with formation of an enolized acetate, Figure 7, can be considered as a fundamental step in the subsequent reactivity of the adsorbed species. The reaction can take various routes, and only a few of them have been explored so far, in particular for ZrO_2 surfaces, due to the large computational costs involved. The complexity of the reaction has limited the investigations to the most stable surfaces of zirconia. To date, calculations on ketonization reactions have not been reported for titania surfaces, and also the role of extended defects or the presence of excess electrons (Ti^{3+}, Zr^{3+}) has not been investigated.

The reasons why prereduction treatments and metal deposition result in an increased activity in ketonization processes[22] are not entirely clear. In particular, the role of supported metal particles (e.g., Ru) remains elusive. In a recent DFT study, it was shown that Ru nanoclusters containing up to 10 atoms interact with the (101) surface of anatase TiO_2 leading to a partial charge transfer from the metal to the oxide.[110] One could speculate that the presence of extra charge on the oxide surface can be beneficial for the activation and dissociation of the carboxylic acids. However, it is also possible that the metal nanoparticles have only an indirect effect, like for instance favoring H_2 dissociation in prereduction treatments of the catalysts; hydrogen atoms then spill over from the metal particle to the oxide surface where they split into protons, adsorbed on the surface O ions, and electrons that reduce Ti and Zr ions from the +4 to the +3 oxidation state. But one cannot exclude other hypotheses related to the presence of supported metals: for exampe, they can stabilize existing defects like anion vacancies or promote their migration toward the surface, they can react with the oxide support with formation of oxide nanoclusters (e.g., Ru_xO_y) or encapsulated core−shell nanoparticles, or they can induce the diffusion and penetration into the oxide material of individual metal atoms which result in interstitial (or even substitutional) doping, an effect which is know to alter significantly the properties of a catalyst.[111,112] None of these possibilities has been explored so far, leaving ample space for future investigations based on DFT studies.

AUTHOR INFORMATION

Corresponding Author

*E-mail: gianfranco.pacchioni@unimib.it. Tel.: +39-2-64485219.

Notes

The authors declare no competing financial interest.

ACKNOWLEDGMENTS

I thank D. Serrano and D. E. Resasco for their critical reading of the manuscript. This work has been supported by the European Community's Seventh Framework Programme FP7/2007-2013 under Grant Agreement n° 604307 (CAS-CATBEL) and by Italian MIUR through the FIRB Project RBAP115AYN "Oxides at the nanoscale: multifunctionality and applications". The support of the COST Action CM1104 "Reducible oxide chemistry, structure and functions" is also gratefully acknowledged.

REFERENCES

(1) Mohan, D.; Pittman, C. U.; Steele, P. H. *Energy Fuels* **2006**, *20*, 848−889.
(2) Bertero, M.; de la Puente, G.; Sedran, U. *Fuel* **2012**, *95*, 263−271.
(3) Vispute, T. P.; Zhang, H.; Sanna, A.; Xiao, R.; Huber, G. W. *Science* **2010**, *330*, 1222−1227.
(4) Shen, W.; Tompsett, G. A.; Xing, R.; Conner, W. C., Jr.; Huber, G. W. *J. Catal.* **2012**, *286*, 248−259.
(5) Barteau, M. A. *Chem. Rev.* **1996**, *96*, 1413−1430.
(6) Rajadurai, S. *Catal. Rev.: Sci. Eng.* **1994**, *36*, 385−403.
(7) Patai, S. *The Chemistry of the Carbonyl Group*; Interscience, London, 1966.
(8) Pham, T. N.; Sooknoi, T.; Crossley, S. P.; Resasco, D. E. *ACS Catal.* **2013**, *3*, 2456−2473.
(9) Martinez, R.; Huff, M. C.; Barteau, M. A. *J. Catal.* **2004**, *222*, 404−409.
(10) Nguyen, M. T.; Sengupta, D.; Raspoet, G.; Vanquickenborne, L. G. *J. Phys. Chem.* **1995**, *99*, 11883−11888.
(11) Kijenski, J.; Glinski, M.; Jakubowski, A. *Appl. Catal., A* **1995**, *128*, 209−217.
(12) Pestman, R.; Koster, R. M.; van Duijne, A.; Pieterse, J. A. Z.; Ponec, V. *J. Catal.* **1997**, *168*, 265−272.
(13) Sugiyama, S.; Sato, K.; Yamasaki, S.; Kawashiro, K.; Hayashi, H. *Catal. Lett.* **1992**, *14*, 127−133.
(14) Kuriacose, J. C.; Jewur, S. S. *J. Catal.* **1977**, *50*, 330−341.
(15) Pestman, R.; van Duijne, A.; Pieterse, J. A. Z.; Ponec, V. *J. Mol. Catal. A* **1995**, *103*, 175−180.
(16) Kim, K. S.; Barteau, M. A. *J. Catal.* **1990**, *125*, 353−375.
(17) Okumura, K.; Iwasawa, Y. *J. Catal.* **1996**, *164*, 440−448.
(18) Renz, M. *Eur. J. Org. Chem.* **2005**, 979−988.
(19) Ignatchenko, A.; Kozliak, E. *ACS Catal.* **2012**, *2*, 1555−1562.
(20) Yamada, Y.; Segawa, M.; Sato, F.; Kojima, T.; Sato, S. *J. Mol. Catal. A* **2011**, *346*, 79−86.
(21) Nagashima, O.; Sato, S.; Takahashi, R.; Sodesawa, T. *J. Mol. Catal. A* **2005**, *227*, 231−239.
(22) Pham, T. N.; Shi, D.; Sooknoi, T.; Resasco, D. E. *J. Catal.* **2012**, *295*, 169−178.
(23) Burke, K. *J. Chem. Phys.* **2012**, *136*, 150901.
(24) Grimme, S. *Wiley Interdiscip. Rev.: Comput. Mol. Sci.* **2011**, *1*, 211−228.
(25) Kohn, W.; Sham, L. J. *Phys. Rev.* **1965**, *140*, 1133−1138.
(26) Perdew, J. P.; Kurth, S. In *A Primer in Density Functional Theory*; Fiolhais, C., Nogueira, F., Marques, M., Eds.; Springer: Berlin Heidelberg, 2003; pp 1−55.
(27) Perdew, J. P.; Chevary, J. A.; Vosko, S. H.; Jackson, K. A.; Pederson, M. R.; Singh, D. J.; Fiolhais, C. *Phys. Rev. B* **1992**, *46*, 6671−6687.
(28) Perdew, J. P.; Burke, K.; Ernzerhof, M. *Phys. Rev. Lett.* **1996**, *77*, 3865−3868.
(29) Hammer, B.; Hansen, L. B.; Nørskov, J. K. *Phys. Rev. B* **1999**, *59*, 7413−7421.
(30) Pacchioni, G. *J. Chem. Phys.* **2008**, *128*, 182505.
(31) Becke, A. D. *J. Chem. Phys.* **1993**, *98*, 5648−5652.
(32) Lee, C. T.; Yang, W. T.; Parr, R. G. *Phys. Rev. B* **1988**, *37*, 785−789.
(33) Perdew, J. P.; Wang, Y. *Phys. Rev. B* **1986**, *33*, 8800−8802.
(34) Perdew, J. P.; Burke, K. *J. Chem. Phys.* **1996**, *105*, 9982−9985.
(35) Adamo, C.; Barone, V. *J. Chem. Phys.* **1999**, *110*, 6158−6170.
(36) Ernzerhof, M.; Scuseria, G. E. *J. Chem. Phys.* **1999**, *110*, 5029−5036.
(37) Heyd, J.; Scuseria, G. E.; Ernzerhof, M. *J. Chem. Phys.* **2003**, *118*, 8207−8215.
(38) Heyd, J.; Scuseria, G. E.; Ernzerhof, M. *J. Chem. Phys.* **2006**, *124*, 219906 (E).
(39) Krukau, A. V.; Vydrov, O. A.; Izmaylov, A. F.; Scuseria, G. E. *J. Chem. Phys.* **2006**, *125*, 224106.
(40) Dovesi, R.; Saunders, V. R.; Roetti, C.; Orlando, R.; Zicovich-Wilson, C. M.; Pascale, F.; Civalleri, B.; Doll, K.; Harrison, N. M.;

Bush, I. J.; D'Arco, Ph.; Llunell, M. *CRYSTAL09 User's Manual*; University of Torino: Torino, Italy, 2009.
(41) Paier, J.; Marsman, M.; Kresse, G. *J. Chem. Phys.* **2007**, *127*, 024103.
(42) Paier, J.; Marsman, M.; Hummer, K.; Kresse, G.; Gerber, I. C.; Angyan, J. G. *J. Chem. Phys.* **2006**, *124*, 154709.
(43) Paier, J.; Marsman, M.; Hummer, K.; Kresse, G.; Gerber, I. C.; Angyan, J. G. *J. Chem. Phys.* **2006**, *125*, 249901.
(44) Todorova, T.; Seitsonen, A. P.; Hutter, J.; Kuo, I. F. W.; Mundy, C. J. *J. Phys. Chem. B* **2006**, *110*, 3685−3691.
(45) Anisimov, V. I.; Aryasetiawan, F.; Lichtenstein, A. I. *J. Phys.: Condens. Matter* **1997**, *9*, 767−808.
(46) Dudarev, S. L.; Botton, G. A.; Savrasov, S. Y.; Humphreys, C. J.; Sutton, A. P. *Phys. Rev. B* **1998**, *57*, 1505−1509.
(47) Hu, Z.; Metiu, H. *J. Phys. Chem. C* **2011**, *115*, 5841−5845.
(48) Marom, N.; Tkatchenko, A.; Rossi, M.; Gobre, V. V.; Hod, O.; Scheffler, M.; Kronik, L. *J. Chem. Theory Comput.* **2011**, *7*, 3944−3951.
(49) Zhao, Y.; Truhlar, D. G. *J. Chem. Phys.* **2006**, *125*, 194101.
(50) Getsoian, A. B.; Bell, A. T. *J. Phys. Chem. C* **2013**, *117*, 25562−25578.
(51) Rahe, P.; Nimmrich, M.; Nefedov, A.; Naboka, M.; Wöll, C.; Kühnle, A. *J. Phys. Chem. C* **2009**, *113*, 17471−17478.
(52) Grätzel, M. *Nature* **2001**, *414*, 338−344.
(53) Yaghi, O. M.; O'Keeffe, M.; Ockwig, N. W.; Chae, H. K.; Eddaoudi, M.; Kim, J. *Nature* **2003**, *423*, 705−714.
(54) McGill, P. R.; Idriss, H. *Surf. Sci.* **2008**, *602*, 3688−3695.
(55) Ojamaee, L.; Aulin, C.; Pedersen, H.; Kaell, P.-O. *J. Colloid Interface Sci.* **2006**, *296*, 71−78.
(56) Grinter, D. C.; Nicotra, M.; Thornton, G. *J. Phys. Chem. C* **2012**, *116*, 11643−11651.
(57) Heckel, W.; Elsner, B. A. M.; Schulz, C.; Müller, S. *J. Phys. Chem. C* **2014**, *118*, 10771−10779.
(58) Nilsing, M.; Persson, P.; Ojamäe, L. *Chem. Phys. Lett.* **2005**, *415*, 375−380.
(59) Sánchez, V. M.; de la Llave, E.; Scherlis, D. A. *Langmuir* **2011**, *27*, 2411−2419.
(60) Spreafico, C.; Schiffmann, F.; VandeVondele, J. *J. Phys. Chem. C* **2014**, *118*, 6251−6260.
(61) Mosconi, E.; Selloni, A.; De Angelis, F. *J. Phys. Chem. C* **2012**, *116*, 5932−5940.
(62) De Angelis, F.; Fantacci, S.; Gebauer, R. *J. Phys. Chem. Lett.* **2011**, *2*, 813−817.
(63) Milman, V.; Winkler, B.; White, J. A.; Pickard, C. J.; Payne, M. C.; Akhmatskaya, E. V.; Nobes, R. H. *Int. J. Quantum Chem.* **2000**, *77*, 895−910.
(64) Diebold, U. *Surf. Sci. Rep.* **2003**, *48*, 53−229.
(65) Vohs, J. M. *Chem. Rev.* **2013**, *113*, 4136−4163.
(66) Quah, E. L.; Wilson, J. N.; Idriss, H. *Langmuir* **2010**, *26*, 6411−6417.
(67) Miller, K. L.; Musgrave, C. B.; Falconer, J. L.; Medlin, J. W. *J. Phys. Chem. C* **2011**, *115*, 2738−2749.
(68) Vittadini, A.; Selloni, A.; Rotzinger, F.; Gratzel, M. *J. Phys. Chem. B* **2000**, *104*, 1300−1306.
(69) Luschtinetz, R.; Gemming, S.; Seifert, G. *Eur. Phys. J. Plus* **2011**, *126*, 98−111.
(70) Pei, Z.-F.; Ponec, V. *Appl. Surf. Sci.* **1996**, *103*, 171−182.
(71) Ariga, H.; Taniike, T.; Morikawa, H.; Tero, R.; Kondoh, H.; Iwasawa, Y. *Chem. Phys. Lett.* **2008**, *454*, 350−354.
(72) Ignatchenko, A. V. *J. Phys. Chem. C* **2011**, *115*, 16012−16018.
(73) Panchenko, V. N.; Zaytseva, Yu.A.; Simonov, M. N.; Simakova, I. L.; Paukshtis, E. A. *J. Mol. Catal. A* **2014**, *388*−*389*, 133−140.
(74) Leger, J. M.; Tomaszewski, P. E.; Atouf, A.; Pereira, A. S. *Phys. Rev. B* **1993**, *47*, 14075.
(75) Kisi, E. H.; Howard, C. J. *Key Eng. Mater.* **1998**, *1*, 153−154.
(76) Dash, L. K.; Vast, N.; Baranek, P.; Cheynet, M.-C.; Reining, L. *Phys. Rev. B* **2004**, *70*, 245116.
(77) Shukla, S.; Seal, S. *Int. Mater. Rev.* **2005**, *50*, 45−64.
(78) Dwivedi, A.; Cormack, A. N. *Philos. Mag.* **1990**, *61*, 1−22.
(79) Parida, K.; Mishra, H. K. *J. Mol. Catal. A* **1999**, *139*, 73−80.
(80) Kresse, G.; Hafner, J. *Phys. Rev. B* **1993**, *47*, 558−561.
(81) Kresse, G.; Furthmüller, J. *Phys. Rev. B* **1996**, *54*, 11169−11186.
(82) Hammaecher, C.; Paul, J.-F. *J. Catal.* **2013**, *300*, 174−182.
(83) Eischens, R. P. *Science* **1964**, *146*, 486−493.
(84) Delley, B. *J. Chem. Phys.* **2000**, *113*, 7756−7764.
(85) Clark, J. M.; Nimlos, M. R.; Robichaud, D. J. *J. Phys. Chem. A* **2014**, *118*, 260−274.
(86) Frisch, M. J.; Trucks, G. W.; Schlegel, H. B.; Scuseria, G. E.; Robb, M. A.; Cheeseman, J. R.; Scalmani, G.; Barone, V.; Mennucci, B.; Petersson, G. A.; Nakatsuji, H.; Caricato, M.; Li, X.; Hratchian, H. P.; Izmaylov, A. F.; Bloino, J.; Zheng, G.; Sonnenberg, J. L.; Hada, M.; Ehara, M.; Toyota, K.; Fukuda, R.; Hasegawa, J.; Ishida, M.; Nakajima, T.; Honda, Y.; Kitao, O.; Nakai, H.; Vreven, T.; Montgomery, J. A., Jr.; Peralta, J. E.; Ogliaro, F.; Bearpark, M.; Heyd, J. J.; Brothers, E.; Kudin, K. N.; Staroverov, V. N.; Kobayashi, R.; Normand, J.; Raghavachari, K.; Rendell, A.; Burant, J. C.; Iyengar, S. S.; Tomasi, J.; Cossi, M.; Rega, N.; Millam, J. M.; Klene, M.; Knox, J. E.; Cross, J. B.; Bakken, V.; Adamo, C.; Jaramillo, J.; Gomperts, R.; Stratmann, R. E.; Yazyev, O.; Austin, A. J.; Cammi, R.; Pomelli, C.; Ochterski, J. W.; Martin, R. L.; Morokuma, K.; Zakrzewski, V. G.; Voth, G. A.; Salvador, P.; Dannenberg, J. J.; Dapprich, S.; Daniels, A. D.; Farkas, O.; Foresman, J. B.; Ortiz, J. V.; Cioslowski, J.; Fox, D. J. *Gaussian 09*, revision B01; Gaussian, Inc.: Wallingford, CT, 2009.
(87) Zhao, Y.; Truhlar, D. *Theor. Chem. Acc.* **2008**, *120*, 215−241.
(88) Clark, J.; Call, S. T.; Austin, D. E.; Hansen, J. C. *J. Phys. Chem. A* **2010**, *114*, 6534−6541.
(89) Bamford, C. H.; Dewar, M. J. S. *J. Chem. Soc.* **1949**, 2877−2882.
(90) Duan, X.; Page, M. *J. Am. Chem. Soc.* **1995**, *117*, 5114−5119.
(91) Gonzalez, F.; Munuera, G.; Prieto, J. A. *J. Chem. Soc., Faraday Trans. 1* **1978**, *74*, 1517−1529.
(92) Pulido, A.; Oliver-Tomas, B.; Renz, M.; Boronat, M.; Corma, A. *ChemSusChem* **2013**, *6*, 141−151.
(93) Grimme, S.; Antony, J.; Ehrlich, S.; Krieg, H. *J. Chem. Phys.* **2010**, *132*, 154104.
(94) Berenblyum, A. S.; Podoplelova, T. A.; Shamsiev, R. S.; Katsman, E. A.; Danyushevsky, V. Ya. *Petrol. Chem.* **2011**, *51*, 336−341.
(95) Laikov, D. N. *Chem. Phys. Lett.* **1997**, *281*, 151−156.
(96) Laikov, D. N.; Ustynyuk, Yu. A. *Russ. Chem. Bull.* **2005**, *54*, 820−826.
(97) Pacchioni, G.; Freund, H. J. *Chem. Rev.* **2013**, *113*, 4035−4072.
(98) Pacchioni, G. *Phys. Chem. Chem. Phys.* **2013**, *15*, 1737−1757.
(99) McEntee, M.; Tang, W.; Neurock, M.; Yates, J. T. *J. Am. Chem. Soc.* **2014**, *136*, 5116−5120.
(100) Molina, L. M.; Hammer, B. *Phys. Rev. Lett.* **2003**, *90*, 206102.
(101) Sicolo, S.; Giordano, L.; Pacchioni, G. *J. Phys. Chem. C* **2009**, *113*, 10256−10263.
(102) Pham, T. N.; Shi, D.; Resasco, D. E. *Topics Catal.* **2014**, *57*, 706−714.
(103) Pham, T. N.; Shi, D.; Resasco, D. E. *J. Catal.* **2014**, *314*, 149−158.
(104) Hendren, T. S.; Dooley, K. M. *Catal. Today* **2003**, *85*, 333−351.
(105) Zaytseva, Yu.A.; Panchenko, V. N.; Simonov, M. N.; Shutilov, A. A.; Zenkovets, G. A.; Renz, M.; Simakova, I. L.; Parmon, V. N. *Topics Catal.* **2013**, *56*, 846−855.
(106) Di Valentin, C.; Pacchioni, G.; Selloni, A. *J. Phys. Chem. C* **2009**, *113*, 20543−20552.
(107) Gionco, C.; Paganini, M. C.; Giamello, E.; Burgess, R.; Di Valentin, C.; Pacchioni, G. *Chem. Mater.* **2013**, *25*, 2243−2253.
(108) Di Valentin, C.; Rosa, M.; Pacchioni, G. *J. Am. Chem. Soc.* **2012**, *134*, 14086−14098.
(109) Giordano, L.; Pacchioni, G. *Acc. Chem. Res.* **2011**, *44*, 1244−1252.

(110) Zhang, S. T.; Li, C.-M.; Yan, H.; Wei, M.; Evans, D. G.; Duan, X. *J. Phys. Chem. C* **2014**, *118*, 3514−3522.
(111) McFarland, E. W.; Metiu, H. *Chem. Rev.* **2013**, *113*, 4391−4427.
(112) Shao, X.; Prada, S.; Giordano, L.; Pacchioni, G.; Nilius, N.; Freund, H.-J. *Angew. Chem., Int. Ed.* **2011**, *50*, 11525−11527.